J. Membrane Biol. 157, 215–230 (1997)

The Journal of
Membrane
Biology

Enhanced Closed-state Inactivation in a Mutant Shaker K^+ Channel

R.K. Ayer, Jr.*, F.J. Sigworth
Department of Cellular and Molecular Physiology, Yale University School of Medicine, 333 Cedar Street, New Haven, CT 06520, USA

Received: 16 December 1996/Revised: 5 February 1997

Abstract. Many mutations that shift the voltage dependence of activation in *Shaker* channels cause a parallel shift of inactivation. The I2 mutation (L382I in the *Shaker* B sequence) is an exception, causing a 45 mV activation shift with only a 9 mV shift of inactivation midpoint relative to the wildtype (WT) channel. We compare the behavior of WT and I2 *Shaker* 29-4 channels in macropatch recordings from *Xenopus* oocytes. The behavior of WT channels can be described by both simple and detailed kinetic models which assume that inactivation proceeds only from the open state. The behavior of I2 channels requires that they inactivate from closed states as well, a property characteristic of voltage-gated sodium channels. A detailed ''multiple-state inactivation'' model is presented that describes both activation and inactivation of I2 channels. The results are consistent with the view that residue L382 is associated with the receptor for the inactivation particles in *Shaker* channels.

Key words: Ion channel — Inactivation — Patch clamp — Kinetic model

Introduction

The Drosophila *Shaker* gene encodes a potassium channel which responds to membrane depolarization by opening and then inactivating. Initial analysis of *Shaker* channel inactivation showed that multiple inactivation mechanisms exist (Iverson & Rudy, 1990; Zagotta & Aldrich, 1990). Two inactivation processes, ''N-type'' and ''C-type,'' have been assigned to separate structural domains of the channel based on genetic (Hoshi, Zagotta & Aldrich, 1991) and pharmacological (Choi, Aldrich & Yellen, 1991) evidence, and interactions between these processes have been characterized (Baukrowitz & Yellen, 1995). In several respects the N-type inactivation process appears similar to an ''open-channel block'' mechanism. The development of inactivation can be accounted for by a voltage-independent transition which occurs only after the channel opens (Zagotta, Hoshi & Aldrich, 1989; Hoshi, Zagotta & Aldrich, 1990), and recovery from inactivation often occurs through the open state as well (Demo & Yellen, 1991; Ruppersberg et al., 1991). This behavior contrasts with that of the voltage-gated sodium channel, where the development of inactivation can clearly occur from closed states of the channel, and where channel reopening on recovery from inactivation is very rare (Kuo & Bean, 1994). In the present study we characterize a mutation of the *Shaker* channel which changes the inactivation process, making it functionally more similar to that of sodium channels.

The cytoplasmic linker between transmembrane segments S4 and S5 has previously been shown to be involved in inactivation and is thought to contain the binding site for the N-terminal inactivation particle (Isacoff, Jan & Jan, 1991). The point mutation I2 described in the present study lies immediately adjacent to the linker at the end of the S4 region. The mutation substitutes an isoleucine for leucine residue L370 of the Shaker 29-4 variant; to avoid confusion with other work, we refer to this residue as L382, which is the corresponding position in the more familiar ShB sequence. Earlier physiological analysis of substitutions at L382 demonstrated positive shifts in the voltage dependence of activation (McCormack, Lin & Sigworth, 1993). As expected in a channel where inactivation is strongly coupled to channel opening, the shifts in activation due to various substitutions were paralleled by shifts in the voltage dependence of inactivation. In two-microelectrode voltage clamp recordings, the inactivation midpoint voltage V_h was seen to be typically 30 mV negative to the activation midpoint

* *Present address:* Department of Molecular and Cell Biology, University of California, Berkeley, CA 94720

Correspondence to: F.J. Sigworth

V_{act}, as shown in Fig. 1. The I2 mutation however is exceptional; for this substitution, V_h is 50 mV negative to V_{act}.

In this report we show how the biophysical properties of I2 are changed with respect to wildtype. We first compare the equilibrium and kinetic behavior of inactivation in these channels with the predictions of two simple theories of open-state inactivation. We then compare changes in peak currents due to enzymatic removal of N-type inactivation. Finally we evaluate specific kinetic models of the *Shaker* gating processes which include either open-state inactivation or a combination of open and closed-state inactivation processes.

Materials and Methods

Construction of cDNA Templates and Preparation of mRNA

The construction of the cDNA templates used in this study is described by McCormack et al. (1993). The wildtype (WT) *Shaker* that we use (*Shaker* 29-4; Kamb, Tseng-Crank & Tanouye, 1988) differs from the more widely used ShB splice variant (Schwarz et al., 1988) in its amino terminus and at four residues in the C-terminal region; it has a slightly slower rate of N-type inactivation. The I2 mutant (McCormack et al., 1993) is in the 29-4 background and consists of an isoleucine substitution for L370, which is the second leucine in the leucine heptad repeat (McCormack et al., 1991). Also used in this study were genetically truncated versions of the wildtype and I2 cDNAs (denoted WTT and I2T respectively). In these constructs, residues 2–30 of the amino terminus were removed from WT and I2 to eliminate N-type inactivation. All cDNA constructs were inserted into the vector pGEM (Promega, Madison WI) which was modified to append a poly-A tail to the inserted cDNA (McCormack, Joiner & Heinemann, 1994). Use of constructs with a poly-A tail greatly increased expression in oocytes. mRNAs were transcribed from the cDNA templates as described (McCormack et al., 1993) and stored in RNAse free water at −70°C.

Oocyte Expression

Xenopus oocytes were harvested from female frogs which had been anesthetized using topical application of 0.14% 3-amino benzoic acid methyl ester. Ovarian lobes were digested for 2–3 h in collagenase 1A (Sigma, 2 mg/ml) in OR-3. OR-3 is 50% Leibowitz L15 (GIBCO), 15 mM HEPES, 50 units/ml Nystatin (Sigma), 2μg/ml Gentamycin (Sigma), pH 7.4. After digestion, oocytes were thoroughly washed and stored at 17°C in additional OR-3. The following day, mature oocytes (stage V and VI) were selected for injection. We injected 50 nl mRNA at concentration ranges chosen to produce 100 to 1,000 pA currents in macropatches. Prior to macropatch recording, current levels were checked using a two-microelectrode voltage clamp. We found that 10 to 100 μA levels of current in whole oocytes generally corresponded to macropatch currents in the range desired. Voltage clamping was done in a bath containing OR-3 or ND96 (in mM: 96 NaCl, 2 KCl, 1.8 $CaCl_2$, 1 $MgCl_2$ and 5 HEPES, pH 7.5).

Macropatch Recording

Recording of currents in inside-out macropatches followed standard procedures (McCormack et al., 1993; Rudy & Iverson, 1992). For removal of the vitelline membrane an oocyte was transferred to a hypertonic medium which contained (in mM): 200 K-Aspartate, 20 KCl, 10 EGTA, 1 MgCl2, 10 HEPES, pH 7.4. The vitelline membrane was removed with fine forceps as quickly as possible to minimize time in this solution. The oocyte was subsequently transferred to a small (c. 1 ml volume) chamber fixed to an inverted microscope. The chamber contained the solution which would become the intracellular medium after patch excision. In all experiments this solution was, in mM: 139 K-Aspartate, 1 KCl, 1 EGTA, 10 HEPES, pH 7.4.

Patch pipettes were fabricated from 1.2 mm Corning 7052 glass (Garner Glass, Claremont CA), pulled to tip sizes of 1–5 μm, coated with Sylgard and fire polished. Pipettes were filled with one of two different extracellular solutions. With the exception of the trypsin experiments, all experiments used the NMG pipette solution containing (in mM): 120 n-methyl-D-glucamine-Aspartate, 1.8 $CaCl_2$, 10 HEPES, pH 7.4. The trypsin experiments used the Na pipette solution containing (in mM): 120 Na-Aspartate, 1.8 $CaCl_2$, 10 HEPES, pH 7.4. The NMG pipette solution produced a liquid junction potential of −10 mV; membrane potential values were corrected for this.

Early experiments were done in external NMG-Aspartate solution to follow as closely as possible the recording conditions used in experiments which constrained the kinetic model that we used. The faster C-type inactivation seen in external NMG^+ compared to external Na^+ (Lopez-Barneo et al., 1993), raises the possibility that C-type inactivation might become fast enough to confound the effects of N-type inactivation. A comparison of the rates of inactivation in NMG solutions however shows that C-type inactivation is relatively slow, decaying in 200–500 msec in both WTT and I2T channels, while N-type inactivation yields current decays in 5-10 msec. In K^+-free external solutions C-type inactivation follows very rapidly after N-type inactivation (Baukrowitz & Yellen, 1995), but does not affect its kinetics.

Trypsin (Sigma) was prepared at a concentration of 25 mg/ml in distilled water and stored at −20°C in 100 μl aliquots. Thawed just before use, the enzyme was applied to the intracellular side of excised patches by adding a 1 μl bolus of the 25 mg/ml stock to the bath near the patch pipette. As the bath had a volume of 1 ml, the nominal final concentration of trypsin was 25 μg/ml (Hoshi et al., 1990). As trypsin was added as a bolus there may have been initially higher concentrations in the area of addition. Generally several minutes passed before any removal of fast inactivation was observed; full removal of inactivation took roughly an additional minute. In one patch, the removal of inactivation occurred within 15 sec, suggesting that application had in this case occurred very close to the patch membrane. Conversely, in roughly a third of all patches, there was no effect seen in 5–10 min after application of trypsin and in these cases an additional bolus was added. Trypsin always eventually removed inactivation if the patch survived multiple applications. These dynamics suggest that the concentration of trypsin used was sufficient but not greatly in excess of the amount necessary to remove inactivation. To minimize expected nonspecific effects of enzyme on the channel proteins, current records were obtained as soon as fast inactivation had been removed; the current was stable over 5 to 10 min. Once the recording chamber and oocyte were exposed to trypsin, the oocyte was discarded and the chamber was thoroughly rinsed before further experimentation.

Patch recording employed an EPC-9 patch clamp amplifier under the control of the Acquire software (HEKA Electronic, Lambrecht, Germany) run on an Atari ST computer. Offline analysis was done with the Review program (Instrutech, Mineola, NY) and our own software running on Macintosh computers. Leak currents were subtracted by use of the P/4 protocol (Bezanilla & Armstrong, 1977). The interval between depolarizations (typically 5 sec) was chosen to allow complete recovery from inactivation.

To interpret macroscopic current-voltage relationships, the single-open-channel current-voltage relation (*i-V*) must be known. We obtained this relation as follows. The macroscopic instantaneous *I-V* relation was measured from a series of tail currents from non-

inactivating channels. Instantaneous *I-V* curves from eight WT and eight I2 patches were averaged and scaled to match the corresponding single-channel-currents measured at +80 mV. The WT and I2 single channel *i-V*s were nearly identical. To use them in the modeling each was fitted, over the voltage range −150 to +80 mV, to the Goldman-Hodgkin-Katz (GHK) current equation (Hille, 1992):

$$I_K(V) = I_{offset} + C_1 V \frac{[K]_i - C_0 \exp(-C_2 V)}{1 - \exp(-C_2 V)}. \quad (1)$$

Here $[K]_i = 0.14$ M and the other parameters are as follows. For WT: $I_{offset} = -7.1 \times 10^{-14}$ A, $C_o = 10^{-3}$ M, $C_1 = 1.15 \times 10^{-10}$ *S/M*, $C_2 = 2.2\ V^{-1}$; for I2: $I_{offset} = -1.1 \times 10^{-13}$ *A*, $C_o = 10^{-3}$ M., $C_1 = 1.33 \times 10^{-10}$ *S/M*, $C_2 = 2.2\ V^{-1}$. While there was no external potassium in our solutions, the macroscopic instantaneous *I-V* curves did show inward current for both WT and I2 below −120 mV. We assume that this is a function of a small accumulation of potassium, and the constant C_o of 1 mM is introduced to allow for this small inward current in the fits.

The normalized ''conductance'' curves were then obtained as follows: patches were depolarized from a holding potential of −100 mV in 10-mV steps to test potentials throughout the activation range (−60 to +80 mV for WT; −50 to +110 mV for I2). The maximal current during 50 msec test pulses at each voltage was divided by the single-channel current value at the same voltage and the entire curve was normalized to the value obtained at maximal depolarization. The same methodology was used to obtain normalized conductance curves for both inactivating and noninactivating currents with one exception: in the trypsin experiments, both the pre- and post-trypsin conductance-voltage curves were normalized to the maximal conductance in the post-trypsin data. This had the effect of preserving the magnitude of the conductance change due to the removal of inactivation.

The voltage dependence of steady state inactivation was obtained by the method of prepulse inactivation. Patches were depolarized from rest to a variable amplitude prepulse followed by a fixed amplitude test pulse. Prepulses of 100 msec duration to voltages of −110 to +30 mV (WT) or −100 to +40 mV (I2) were followed by 30–50 msec test pulses to voltages which maximally activated the channel (+80 mV for WT; +110 mV for I2). The maximal amplitude of the current during the test pulse was plotted against the prepulse voltage. As a normalization procedure, the current amplitudes from each patch were fitted to a Boltzmann function and the maximal current level of the Boltzmann fit was then used to normalize the currents at all voltages. This normalization procedure appeared to introduce less scatter than the usual normalization by the maximal current.

Nonstationarity Related to Patch Excision

The activation rate of inactivating WT channels increases with time after patch excision. This change is not seen in the nonactivating WTT or I2T channels and is minimal for inactivating I2. For all constructs, immediately after patch excision, we applied a voltage clamp protocol of depolarizations to study activation, followed by a second, prepulse protocol to measure the voltage dependence of steady-state inactivation; by the time the second protocol was run (*c.* 5 min after excision) the increase in WT activation rate had occurred. In the kinetic modeling the rates for WTT, I2T and I2 were constrained using the kinetics of currents generated by the first protocol. For WT however the rates were constrained using the currents recorded during the prepulses of the inactivation protocol. The WT activation rates obtained from these currents were indistinguishable from rates constrained using WTT currents; by contrast, WT rates constrained using the initial protocol were 30% slower in 4 of 6 patches. The I2 activation rate also increased during the first few minutes after patch excision; however, the change in activation rates was smaller (15%) and is within the normal range of patch-to-patch variability in rate constants (*see below*).

Kinetic Modeling

Computer modeling was done on a Macintosh Quadra 840AV computer. Initial comparisons of steady-state behavior and kinetics of partial models were done with a spreadsheet program (Microsoft Excel). Detailed modeling used the program IkFit running in the PowerMod Modula-2 programming environment (HEKA Electronic). This program solves for the time course of the open probability of a channel following an arbitrary series of voltage steps by computing the spectral expansion of the Q matrix at each voltage (Colquhoun & Hawkes, 1995). Each rate constant was assumed to depend exponentially on voltage, e.g.,

$$\alpha_1(V) = \alpha_1(0) e^{\zeta_{\alpha 1} V/kT} \quad (2)$$

where $\zeta_{\alpha 1}$ is the partial charge associated with the rate constant α_1. Parameters were varied either manually or automatically (simplex algorithm) to minimize the least-squares error in fits to families of traces.

Using IkFit, we were able to reach a set of model parameters (listed in Tables 1 and 2) which fit the kinetic data for all patches containing a given construct while allowing only small changes in rate constants to allow for patch-to-patch variability ($\leqslant \pm 20\%$). Alternatively, if we allowed for a small voltage offset while fitting ($\leqslant \pm 5$ mV), the exact rate constants given in the tables applied across many patches. In the fits presented in the figures, the offset is zero and the values of rate constants are those given in Tables 1 and 2 except when noted.

Values of measured parameters are given as mean ± SE in the text.

Results

Wild-Type and I2 Currents

The differential shift of activation and inactivation by the I2 mutation previously observed in whole-oocyte recordings (Fig. 1) is borne out in macropatch recordings where the speed and quality of voltage control is much better. Macropatch currents from oocytes injected with wildtype (WT) or I2 cRNAs are shown in Fig. 2*A* and *C*. Although the currents have similar time courses, several differences in voltage dependence and kinetics can be observed. First, WT patches begin to show current at depolarizations to −50 mV while I2 patches do not show clear activation below −30 mV. The differences in voltage dependence may be more clearly seen in Figs. 2*E* and *F*. While the prepulse inactivation curves for WT and I2 (Fig. 2*E*) show a difference of only 9 mV in the midpoint voltage V_h, the corresponding peak conductance curves (Fig. 2*F*) are displaced by about 32 mV. Second, the inactivation of I2 current is somewhat faster than that of wildtype. At large depolarizations, where the time course becomes voltage-independent, the time constant of WT inactivation is 4.5 msec, while for I2 the value is 3.75 msec. At smaller depolarizations the comparison between the two constructs is more complex. At a given voltage, wildtype inactivation tends to be faster: at −30 mV the time constant of a single-exponential fit is 7.8 msec for WT, 10.1 msec for I2. However, if one looks at similar levels of activation, say −30 mV for WT and +20 mV for I2, the latter decays

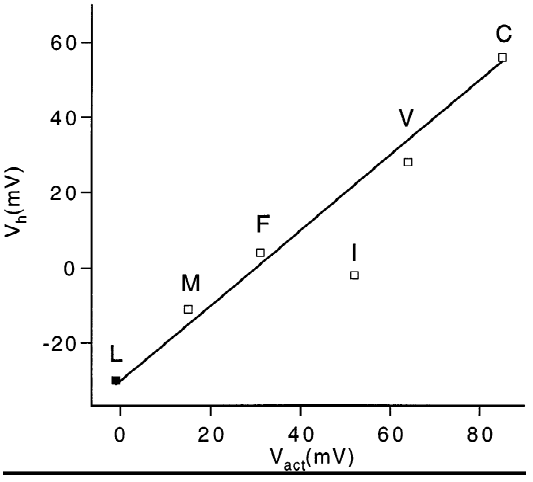

Fig. 1. Correlation of activation and inactivation in substitutions at position 382 of the *Shaker* B sequence. The midpoint voltage of inactivation V_h is plotted as a function of the activation midpoint voltage V_{act} for *Shaker* 29-4 channels with substitutions of the leucine residue at this position. Values were taken from Table 1 of McCormack et al. (1993), determined as the midpoint voltages of Boltzmann fits to prepulse-inactivation and peak-conductance curves from two-microelectrode voltage clamp of *Xenopus* oocytes. The solid line has a slope of unity and represents a displacement between V_{act} and V_h of 30 mV.

much more quickly (7.8 msec for WT, 3.4 msec for I2). Third, the amount of noninactivating, steady-state current present after a long depolarizing stimulus is generally smaller for wildtype than for I2. This can be seen in the largest depolarizations in Fig. 2*A* and *C*. The amount of current remaining at the end of a long voltage pulse was quantified in WT and I2 patches as the fraction of peak current at +70 mV; its average value was .04 ± .01 for WT ($n = 6$) and .07 ± .01 for I2 ($n = 11$).

Removal of N-type inactivation produces currents which inactivate much more slowly (Fig. 2*B* and *D*); again WT current is seen to activate at more negative voltages than I2. In Fig. 2*B* and *D*, N-type inactivation has been removed by trypsin treatment; the kinetics of these currents are indistinguishable from channels whose N-type inactivation has been removed genetically. At a given voltage the currents reach maximal activation at similar times (e.g., 5 msec for both WT and I2 at 0 mV); however at a given fraction of maximal conductance, I2 activates much more quickly. The activation curves of noninactivating channels (Fig. 2*G*) are steeper and shifted to negative voltages compared to those for the inactivating channels (Fig. 2*F*); the difference is most dramatic for WT.

Equilibrium Properties of Inactivation

As demonstrated in Fig. 2, the I2 mutation shifts the voltage dependence of activation to a much greater extent than it shifts the voltage dependence of inactivation. One of the consequences of this differential shift is that the I2 current is almost fully inactivated at potentials that yield quite low levels (15–20%) of current activation. To reach a similar level of inactivation in the wildtype requires activation of greater than 50% of total current. This difference is quantified in Fig. 3*A* by plotting the steady state value of the inactivation parameter h as determined from prepulse experiments, as a function of an activation parameter p_o' at the same voltage. Here p_o' is taken to be the open probability of the channel in the absence of inactivation. The figure demonstrates that over a wide range of p_o' there is more complete inactivation (h is smaller) for I2 currents than for WT currents.

It is possible to predict the relationship between steady state inactivation and activation for channels which inactivate only through the open state. Consider a channel with closed, open and inactivated states

$$C \underset{}{\overset{r_a}{\rightleftharpoons}} O \overset{r_i}{\rightleftharpoons} I$$

where r_a and r_i represent the equilibrium constants between the pairs of states as shown. The open probability p_o' in the absence of inactivation (i.e., with $r_i = 0$) will be

$$p_o' = \frac{r_a}{1 + r_a} \tag{3}$$

For any value of r_i the activatable fraction of channels, that is the probability that a channel will not be in the inactivated state, is

$$h = 1 - \frac{r_a r_i}{1 + r_a + r_a r_i} \tag{4}$$

which can be rewritten using Eq. (3) as

$$h = \frac{1}{1 + r_i p_o'}. \tag{5}$$

The relationship (5) is quite general; it holds also for schemes with multiple steps in the activation process, provided that there is only one open state and that inactivation occurs only from the open state. It thus provides a simple prediction for open-state inactivation. The solid curve in Fig. 3*A* shows a plot of this relationship; the value of r_i was taken to be voltage independent and was determined from the h value at large depolarizations where p_o' approaches unity.

This model of inactivation fails to accurately predict

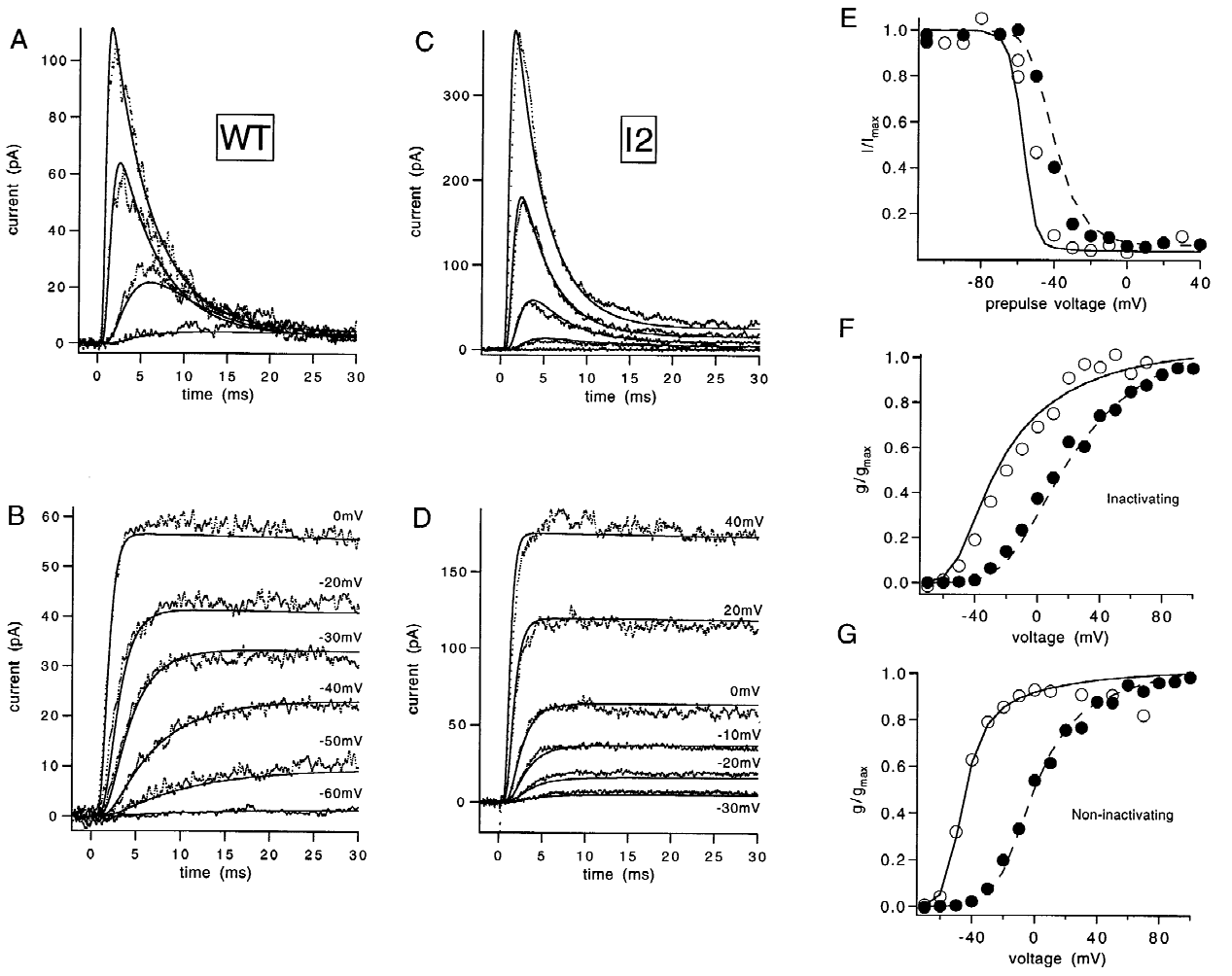

Fig. 2. Macroscopic currents from wildtype and I2 channels. Currents were recorded from inside-out patches containing wildtype (*A, B*) or I2 (*C, D*) channels. Inactivating currents were recorded with NMG pipette solution and a holding potential of −110 mV; depolarizations were to −50, −30, +10, +50 mV in *A;* −40, −20, 0, +30, +70 mV in *C.* Noninactivating currents in panels *B* and *D* were recorded with Na pipette solution and after application of trypsin to the cytosolic side; holding potential was −100 mV. Depolarizations were to −60, −50, −40, −30, −20, 0 mV in *B;* −30, −20, −10, 0, +20, +40 mV in *D.* Filter bandwidth was 2 kHz in A and B; 3 kHz in *C* and *D.* (*E*) Inactivation curves obtained with 100 msec prepulses to the indicated voltages in WT (open symbols; $n = 4$) and I2 (closed symbols; $n = 5$). (*F*) Peak conductance of inactivating currents: WT (open symbols; $n = 6$) and I2 (filled symbols; $n = 11$). (*G*) Peak conductance of noninactivating currents from genetically-truncated channels: WTT (open symbols; $n = 3$) and I2T (filled symbols; $n = 3$). In each panel (*E, F* and *G*) the mean values are plotted from the number of experiments given; all data were recorded with NMG pipette solution. Conductance values were obtained by dividing the peak current by the estimated single-channel current (*see* Materials and Methods) and normalizing to the maximum value. Midpoint voltages, obtained from Boltzmann fits of the inactivation and peak conductance data shown in *E, F* and *G* are as follows: *E,* WT −51 mV, I2 −43 mV; *F,* WT −22 mV, I2 + 10 mV; *G,* WT −46 mV, I2 −2 mV. The smooth curves in each part of the figure were computed from the kinetic scheme of Fig. 7 with the rate constants given in Tables 1 and 2. *A, B, C* and *D* show data from experiment numbers 0129WT, 0118WT, 0316I2 and 0107I2, respectively.

the relationship between h and p'_o for either WT or I2. One problem may have to do with the measurement of steady-state inactivation. The inactivation data shown in Figs. 2*E* and 3*A* were obtained using prepulses of 100-msec duration, which is not sufficiently long to reach steady state for small depolarizations of WT channels. Therefore, the measured values of h for WT will tend to be larger than the true values.

For I2 however, the theory predicts too little inactivation, a discrepancy that cannot be explained by insufficiently long prepulses in the inactivation measurement. The lack of correspondence between data and theory for I2 suggests instead that there may be additional pathways for channel inactivation in I2 that do not involve channel opening, but instead can occur from closed states of the channel.

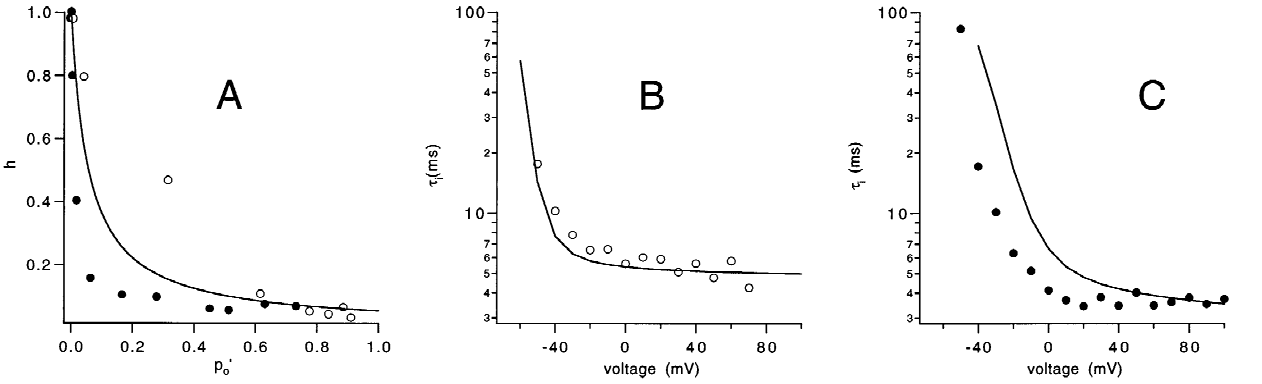

Fig. 3. I2 Inactivation is not well coupled to activation. (*A*) The steady-state inactivation parameter *h* is plotted as a function of the open probability p_o' in the absence of inactivation for WT (open circles) and I2 (closed circles) channels. Values for *h* and p_o' were obtained from Fig. 2*E* and *G* at corresponding voltages. The curve shows the relationship predicted by Eq. (5) with $r_i = 17.5$. (*B*) Voltage dependence of the inactivation time constant τ_i for WT channels. The curve is the prediction of Eq. (6) with $\kappa = 200$ sec^{-1} and $\lambda = 5$ sec^{-1}. (C) Voltage dependence of τ_i for I2 channels. The curve was computed with $\kappa = 320$ sec^{-1} and $\lambda = 10$ sec^{-1}. All data in the figure were obtained using the NMG pipette solution.

Kinetics of Inactivation

A simple model can also make approximate predictions for the kinetics of inactivation. Let inactivation proceed from the open state with rate κ and return with rate λ,

$$C \rightleftharpoons \cdots \rightleftharpoons O \underset{\lambda}{\overset{\kappa}{\rightleftharpoons}} I$$

and let the equilibria among the activation steps be rapid compared to κ and λ. Then the time constant for the decay of the current due to inactivation will be

$$\tau_i \approx \frac{1}{p_o'\kappa + \lambda}. \qquad (6)$$

Thus a measurement of open probability in the absence of inactivation makes a prediction for the inactivation rate. Figure 3*B* and *C* compares the predictions of this model with inactivation time constants for WT and I2 channels. Here κ and λ are taken to be voltage-independent, with their values fixed by the inactivation time constant and fraction of inactivating current at large depolarizations. The behavior of WT channels (Fig. 3*B*) is described by this model as well as can be expected; at threshold potentials the rate of activation of WT channels becomes comparable to κ, so the assumption of rapid activation does not hold there. The inactivation time constant of I2 currents (Fig. 3*C*) is however always much shorter than predicted, a deviation that again suggests that closed-state inactivation may be occurring in I2.

Effects of Removal of Inactivation with Trypsin

As another approach to examine the possibility of closed-state inactivation, we measured the inactivating currents in a macropatch and then applied trypsin to remove N-type inactivation. If closed-state inactivation is occurring to a significant degree in I2, then we expect a larger increase in total current after enzymatic removal of inactivation when compared to WT.

Trypsin has been used previously to remove N-type inactivation from Shaker channels (Hoshi et al., 1990; Gomez-Lagunas & Armstrong, 1995). Neither study documented a change in activation after trypsin treatment though both suggested that a fraction of channels were rendered inoperable by the enzyme. Our experiments rely on a clean removal of inactivation with no effect on activation. As a control, trypsin was applied to WTT and I2T channels which already had N-type inactivation removed through the genetic removal of residues 2–30. In this way, we could determine directly whether enzyme treatment altered *Shaker* activation. Figure 4*A* and *B* shows recordings from a WTT patch. Currents were reduced somewhat, roughly 10% in this patch, but activation kinetics were unaffected by the trypsin treatment. A reduction in current was the only consistent change in two WTT and one I2T patch which received enzyme treatment. Figure 4*C* shows the conductance-voltage data from WT patches of three types: (i) genetically truncated, (ii) genetically truncated and trypsin-treated and (iii) not genetically truncated but trypsin-treated to remove N-type inactivation. The smooth curve is a model prediction (*described below*) of the conductance-voltage relationship. The same curve, and the rates which produce it, describe each of the data sets adequately. Figure 4*D* shows the corresponding conductance-voltage data for I2 channels; again a single curve describes the data satisfactorily. Together these results show that trypsin treatment has little effect on the size of currents or the kinetics or voltage dependence of channel activation.

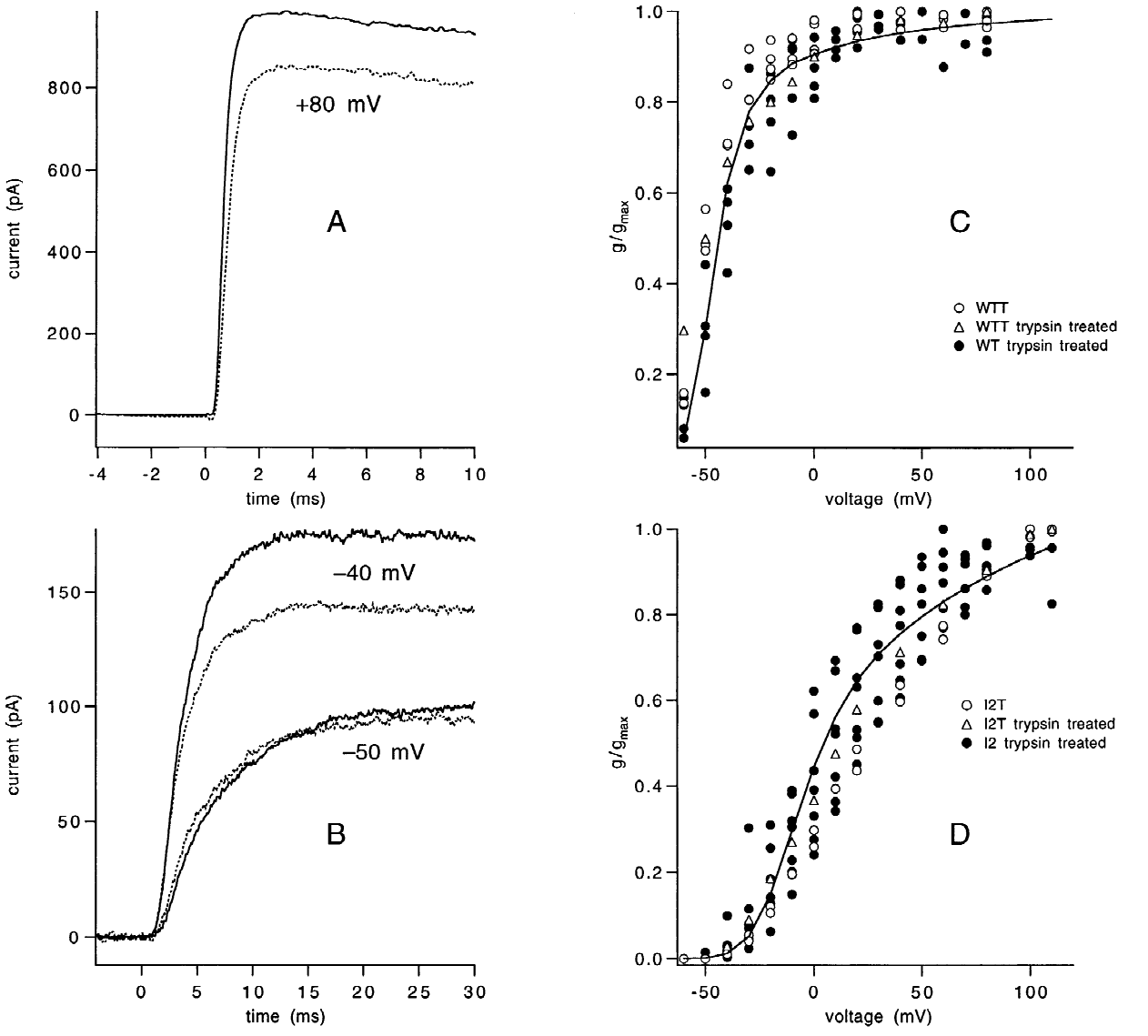

Fig. 4. Trypsin treatment has little effect on *Shaker* activation. (*A, B*) Currents from a patch containing genetically truncated, noninactivating WT channels before (solid curves) and after trypsinization (dotted curves). Depolarizations were applied from a holding potential of −100 mV to the potentials indicated; data were filtered at 3 kHz. (*C*) The voltage dependence of peak conductance is compared in untreated and trypsin-treated WT channels. The open circles are from untreated WTT channels in four experiments; open triangles are from one WTT patch treated with trypsin; closed circles are from trypsin-treated WT channels in four experiments. (*D*) The voltage dependence of peak conductance is compared in untreated and trypsin-treated I2 channels. The open circles are from untreated I2T channels in two experiments; open triangles are from one I2T patch treated with trypsin; closed circles are from trypsin-treated I2 channels in two experiments. The smooth curves in *C* and *D* were computed from the kinetic scheme of Fig. 7 with the rate constants given in Table 1. All data in Fig. 4 were recorded using Na pipette solution.

Figure 5 shows current records from experiments in which trypsin was used to remove inactivation from WT and I2 channels. The panels compare pre- and post-treatment currents for WT (*A*) and I2 (*B*). For each construct is shown currents near threshold (upper panels) and currents at a strong depolarization (lower panels). The change upon trypsin treatment is quite different for the two channel types. For WT, the peak current increase after trypsin application is quite large at threshold (300% increase at −40 mV) but is small at maximal depolarization (17% increase at +60 mV). For I2, the current increase at threshold is smaller (150% at −20 mV) but larger at maximal depolarization (66% increase at +110 mV).

Figure 6 compares the average pre- and post-trypsin conductance-voltage curves for WT and I2 over a wide voltage range. For WT (Fig. 6*A*) the increase in peak current is again seen to be most dramatic with small

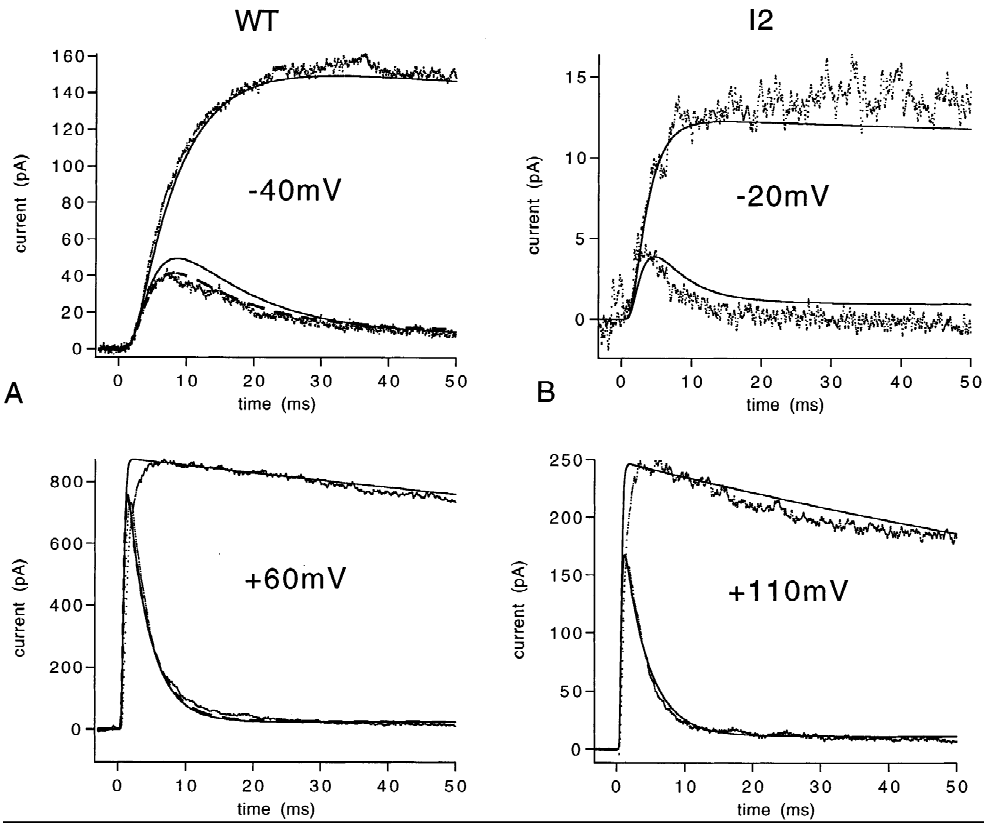

Fig. 5. Trypsin treatment increases the peak current in WT and I2 channels. Currents were recorded from inside out patches containing wildtype (*A*) or I2 (*B*) channels with depolarizations from −100 mV to the potentials shown. Superimposed in each panel are inactivating currents recorded before trypsin, and the larger, noninactivating currents after trypsin treatment. Bandwidth is 3 kHz except for the −20 mV traces in part *B*, where data were filtered to 2 kHz bandwith. The smooth curves overlaying the WT inactivating currents in A are the predictions of the scheme in Fig. 7 using the rate constants in Tables 1 and 2, modified by a voltage shift of −3 mV and scaled to $N = 735$ channels. The smooth curves overlaying the I2 inactivating currents in *B* are the predictions of the corresponding scheme and rate constants but modified by a voltage shift of +3 mV and scaled to $N = 138$ channels. For the effect of trypsin treatment the WT and I2 inactivation rate constants were replaced by slow inactivation from the open state only; the rate constants (sec^{-1}) were: $\kappa = 3$, $\lambda = .015$ (WT) and $\kappa = 5$, $\lambda = .015$ (I2) and the fits were scaled by $N = 685$ channels (WT) and $N = 140$ channels (I2). A second pre-treatment WT prediction in *A*, shown in dashed curves, visible at −40 mV but overlayed by the smooth curve at +60 mV, is generated by the MSI scheme modified by a −3 mV voltage shift and using the inactivation rate constants (sec^{-1}): $\kappa_c = 660$, $\lambda_c = 44$, $a = 4.0$, $\kappa_o = 312$, $\lambda_o = 8.0$ scaled to $N = 761$ channels. *A* and *B* are from experiments 1229 WT and 010612I2 respectively recorded with Na pipette solution.

depolarizations and becomes small at large depolarizations. Such a voltage-dependent increase is to be expected from a channel where the microscopic inactivation rate is voltage independent, and therefore is faster than activation at potentials near threshold and slower than activation at depolarized potentials. This behavior forces the normalized conductance voltage curve of the inactivating current to be shallower and shifted to the right compared to that measured after removal of inactivation. The peak conductance is seen to be still increasing at +80 mV; if inactivation is occurring only from the open state then opening is still not fast enough to allow full activation before inactivation begins to remove open channels.

As can be seen in Fig. 6*B* , trypsin removal of I2 inactivation produces a more uniform increase in current across the entire activation voltage range. On average, trypsin treatment increases currents by 50 to 80% over the voltage range of 30 to 110 mV. The larger increment in current at large depolarizations suggests that an additional inactivation pathway may be reducing the number of available channels before they can open.

Modeling: Adaptation of an Activation Scheme to the I2 Channel

The further characterization of inactivation pathways requires a kinetic model that describes the activation process in detail. Our calculations are based on a preliminary version of the model of Schoppa & Sigworth (1997). This model for nonactivating (NI) *Shaker* channel currents accounts for single-channel, macroscopic ionic and gating currents of WTT *Shaker* channels and

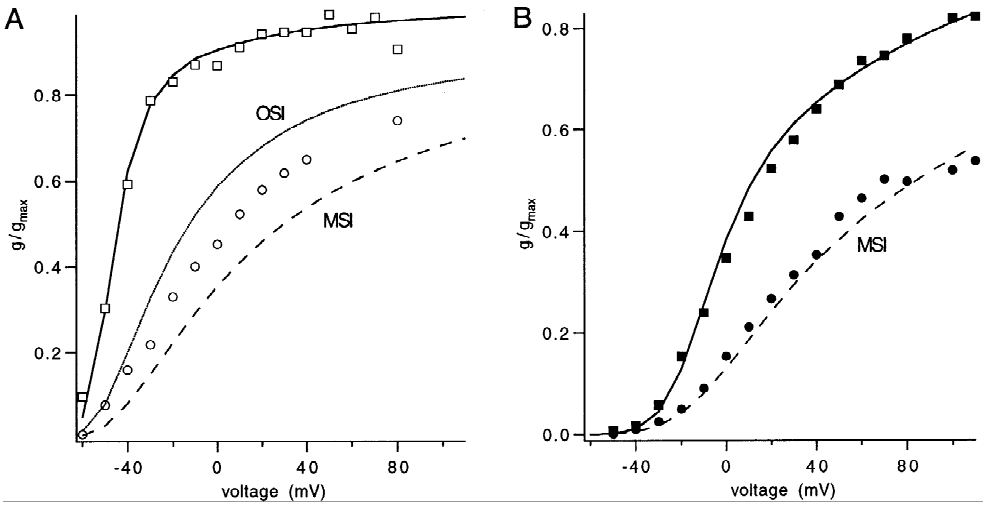

Fig. 6. Voltage dependence of peak conductance before and after trypsin treatment. Plotted are average peak conductance for WT (*A*) and I2 (*B*), before (circles) and after trypsin (squares). Peak conductance from experiments like those shown in Fig. 5 were measured before and after trypsin treatment and normalized to the same value, preserving the change in open probability revealed by the removal of inactivation. Shown are averages across patches ($n = 5$ WT; $n = 7$ I2); all experiments were recorded using Na pipette solution. The solid curves were calculated from the model of Fig. 7 and the WTT and I2T rate constants given in Table 1. The dotted curve in *A* shows the prediction of the OSI scheme fitted to the kinetics of inactivating WT channels using the inactivation rate constants given in Table 2. The dashed curves in both panels are the predictions of the MSI scheme fitted to the kinetics of inactivating WT(A) and I2(B) currents using the inactivation rate constants given in Table 2 for I2 and the following inactivation rate constants for WT (sec^{-1}): $\kappa_c = 660$, $\lambda_c = 44$, $a = 4.0$, $\kappa_o = 312$, $\lambda_o = 8.0$.

also of the V2T mutant (having the mutation L382V in the truncated *Shaker* background). The NI model (Fig. 7*A*) has two main features that distinguish it from other recent models for *Shaker* channel activation (Zagotta, Hoshi & Aldrich, 1994; Bezanilla, Perozo & Stefani, 1994). First, total charge movement and channel gating occurs through a relatively large number of kinetic steps, consisting of three sequential transitions for each of four independent channel subunits. The large number of steps was required by the observed weak voltage dependence of channel kinetics at voltage extremes (Schoppa & Sigworth, 1997). Secondly, the NI model includes two final transitions that lead to channel opening. These concerted transitions serve to impart cooperativity to the system and sharpen the voltage dependence in WTT but not in V2T channels.

As will be shown, I2 inactivation modeling requires inactivation transitions from closed states near the open state. The NI model deals effectively with the kinetics of these final opening transitions for *Shaker* and is the only activation model available which has been constrained using data from a mutation at the L382 position. It is constrained by single channel and gating current measurements in addition to macroscopic ionic currents. Our adaptations of the NI model to the activation of I2T relied on fits to a more limited set of data, consisting only of macroscopic current time courses. Since the voltage dependence of I2T activation lies between that of WTT and V2T, and because the various amino acids substitutions at L382 produce quantitatively similar effects on activation (McCormack, Lin & Sigworth, 1993), we initially changed only those parameters in the NI model which were changed for V2T. These were the rate constants for the final two transitions, particularly the value of δ; no changes in the partial charges ζ were made.

With one exception, detailed in the following paragraph, we found that the kinetics of I2T macroscopic currents were well described by the NI model using activation rates either identical to V2T or intermediate to the values for WTT and V2T (*see* Table 1). Figure 2*B* and *D* shows the ability of the model to fit both I2T and WTT currents whose N-type inactivation has been removed by trypsin; an additional example of the goodness of fit for two other noninactivating patches is shown in the post-trypsin records of Fig. 5.

In one respect, model rates similar to those for either V2T or WTT could not account for I2T behavior. While the midpoint of I2T activation is between the values for WTT and V2T, the slope of the I2T activation curve is shallower than WTT or V2T at large depolarizations (Fig. 8*A; see also* Fig. 1 of McCormack, Lin & Sigworth, 1993). Simple adjustments of the rates leading to channel opening could not reproduce this behavior, but a change in κ_{of} could account for it. The rate constant κ_{of} leads from the open state to the fast-closed state which accounts for single-channel behavior and the weak voltage dependence of open probability at depolarized potentials. It is a rate constant that is unaffected in V2T, but by increasing it by 5 to 10-fold we can account for the shallow activation voltage dependence in I2T.

In the following modeling of inactivating WT and I2 channels, the activation process is constrained from fits

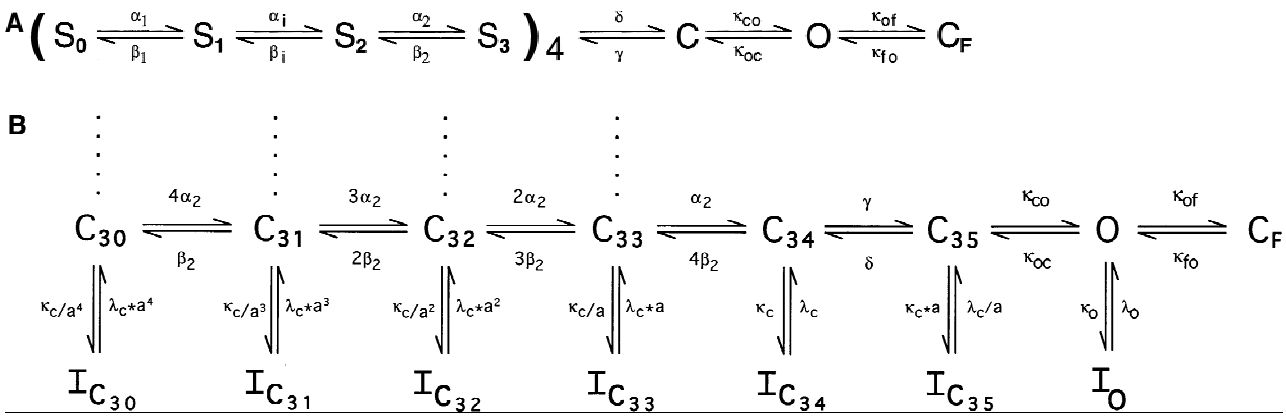

Fig. 7. A kinetic model for WT and I2 channel activation and inactivation. (*A*) A condensed representation of the NI activation scheme. The portion of the scheme in parentheses represents three sequential transitions which occur within each of four independent subunits. The full expansion of this part of the scheme encompasses 34 closed states. After completing these transitions, the channel undergoes two additional concerted transitions before opening. The channel can also enter a fast blocked state, C_f, after opening. Rate constants for WT and I2 are given in Table 1. (*B*) The final states of the activation scheme in *A*, to which inactivation transitions have been added. The OSI model has only inactivation state I_o; the MSI model includes the states I_{C30} through I_{C35} as well. State C_{30} represents the complex when four subunits are in S_2. States C_{31}, C_{32}, C_{33} and C_{34} correspond to the channel after 1, 2, 3 or 4 subunits have completed their final transitions to S_3. The MSI model allows for voltage-independent inactivation transitions from the closed states C_{30} through C_{35} into the inactivated states I_{C30} through I_{C35} respectively. These transitions are more favorable as additional subunits have undergone the final transition, and are most favorable from state C_{35}. Values for the inactivation rate constants are given in Table 2.

to activation kinetics and voltage dependence in the noninactivating WTT and I2T channels. That is to say, no further modification of the NI model, or the rates in Table 1, was allowed when fitting data from the inactivating WT or I2 channels.

Open-state Inactivation Models Account for WT Currents

To produce an open-state inactivation (OSI) model, we added a single transition from the open state of the NI model to the inactivated state I_o (*see* Fig. 7*B*). The transition is governed by voltage independent rates κ_o and λ_o, whose values are listed in Table 2. This scheme was tested to determine its adequacy in describing WT and I2 inactivation. Figure 2*A* shows the fit of the OSI model to currents from a wildtype patch using the rates given in Table 2. The model describes well the currents over this wide voltage range (−50 to +50 mV).

In Fig. 2*F* we show a prediction of the voltage dependence of peak conductance for WT channels from the OSI scheme (solid curve overlaying the average peak conductance in open circles). Both the data and the peak conductance predicted by the model are normalized, so that only the shape of the curve is a test of the model. The curve deviates slightly from the data, tending to predict higher peak conductances at intermediate voltages than are observed.

The OSI model was also used to predict the voltage dependence of steady-state inactivation, as shown as the solid curve in Fig. 2*E*. As can be seen, the OSI model predicts stronger steady-state inactivation than is seen in WT patches. Surprisingly, reducing the open-state inactivation by decreasing κ_o does not correct this discrepancy; however slowing activation slightly (by decreasing all activation rates by about 10%) does produce an excellent fit of the steady-state inactivation curve, with only minor effects on the kinetic aspects of the fit. That inactivation is sensitive to activation rates is a correlate of the strong coupling of the two processes in the OSI model.

When applied to I2 currents, the OSI model can account well for data obtained with large depolarizations, but at threshold and midrange voltages (−40 to +30 mV) the OSI model predicts currents that are too large and decay too slowly. Figure 8*C* demonstrates the good fit of the OSI model to I2 currents at +90 mV, but at −10 mV the same scheme predicts a current (dashed curve in Fig. 8*B*) that is too large and which decays much more slowly than the data. Additionally, the OSI model predicts a steady-state inactivation relation that lies 10–20 mV positive to the observed steady-state inactivation curve (*not shown*). It is possible to speed up inactivation (setting $\kappa_o \approx 1000$ sec^{-1}) to produce faster decays for currents near threshold; however, this makes the current decay much too fast at depolarized potentials. In conclusion, we find that the OSI model is quite successful in predicting WT behavior, but fails to account for I2 behavior.

A Multiple-state Inactivation Model Accounts for Many Aspects of I2 Behavior

The analysis of I2 currents up to this point suggests that I2 lacks the strict coupling of inactivation to channel

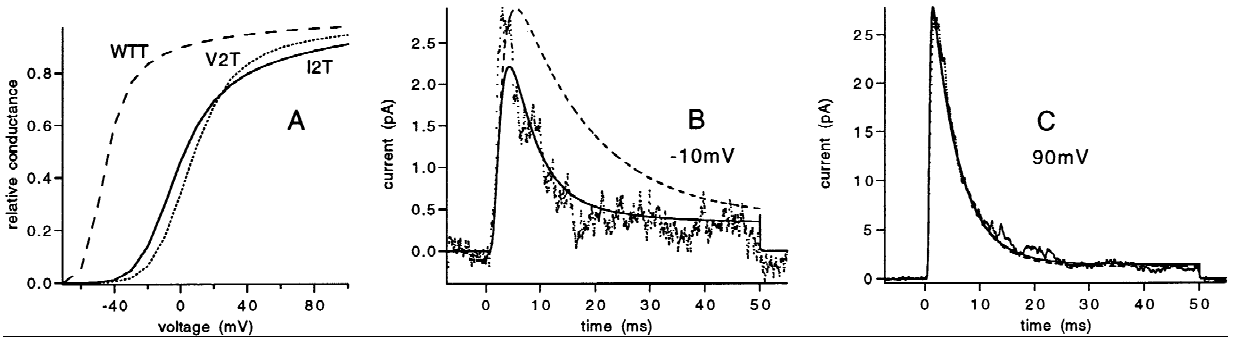

Fig. 8. Examination of the NI, OSI and MSI Models. (*A*) Plotted is the voltage dependence of activation, expressed here as relative conductance, predicted by the NI model for WTT (dashed curve) and the two noninactivating mutants, V2T (dotted curve) and I2T (solid curve). The rate constants used in the NI model are given in Table 1. (*B, C*) Currents recorded from an I2 patch with NMG pipette solution, elicited by steps from a holding potential of −110 mV to −10 mV (*B*) and +90 mV (*C*). The solid curves are the predictions of the model of Fig. 7 using the rate constants given in Table 1, modified by a voltage shift of +3 mV and with the following modification of inactivation rates (sec^{-1}): $\kappa_o = 215$, $\lambda_o = 7.0$. The dashed curves, visible at −10 mV but overlayed by the smooth curve at 90 mV, are produced by an identical scheme and rate constants with the exception that inactivation from the closed states has been removed.

opening that accounts for the behavior of the wildtype channel (Figs. 1, 2 and 3). Enzymatic removal of inactivation seems to uncover a fraction of I2 current that inactivates without channel opening (Fig. 6*B*). The OSI scheme fails to account for the kinetics and steady-state behavior of I2. From these findings it appears likely that the I2 channel is capable of inactivation from states other than the open state. To further test this hypothesis, we extended the kinetic model to include inactivation from several closed states as well as from the open state.

The construction of a closed-state inactivation model was constrained by two considerations. First, if I2 channels could inactivate from closed states far from the open state and near the most closed state, we would not expect to see steady-state inactivation curves that saturate at roughly the same voltages (−60 to −70 mV) as is seen for WT channels. Thus inactivation is expected to occur only from states near the open state. Second, in keeping with the voltage independence of open state inactivation, we assume that inactivation from the closed state is also voltage independent.

The activation model of Zagotta et al. (1994) involves four independent subunits, each of which undergoes two sequential transitions. While this model did not include inactivation transitions, the authors suggested that closed state inactivation might occur after the first sequential transition has occurred in each subunit. Following this suggestion, we chose to allow inactivation transitions to occur from the equivalent closed states in the NI model, states C_{30} through C_{34} (Fig. 7*B*). The rates of inactivation from each of the closed states were allowed to differ because they represent different degrees of activation; this makes mechanistic sense if we imagine that inactivation becomes easier as structures which block the access of an inactivation particle move out of the restrictive position as each subunit moves into its permissive conformation. To minimize free parameters,

Table 1. Activation rate constants

Rate	$\zeta(e_0)$	Rate at 0 mV (s^{-1})		
	WTT, I2T, V2T	WTT	I2T	V2T
α_1	0.47	1438	1438	1438
β_1	−0.5	413	413	413
α_i	0.1	7794	6859	6755
β_i	−0.52	1167	1277	1392
α_2	0.1	5196	3637	3533
β_2	−0.52	778	675	737
γ	0.7	7592	5236	5236
δ	−0.3	446	11138	23167
κ_{co}	0.2	6246	4320	4320
κ_{oc}	−0.55	243	647	647
κ_{of}	0.0	200	2500*	500
κ_{fo}	0.3	3367	3367	3367

* The rate given is for external Na^+ for external NMG^+, the rate is 975 sec^{-1}.

we used a single set of forward and backward rates, κ_C and λ_C for the inactivation transition from C_{34}; transitions from C_{33}, C_{32} C_{31} and C_{30} are made progressively less favorable by scaling the rate constants by factors a and a^{-1}, respectively. C_{34} is the state where I2 closed state inactivation would be expected to be most effective. The large reverse rate constant $\delta = 11100$ sec^{-1} leading from C_{35} into C_{34} and the lower rates leading away from C_{34} (in sec^{-1}: $4\beta_2 = 2700$ and $\gamma = 5230$) lead to a high probability of occupancy of this state at threshold and midrange voltages.

This scheme produced very good fits to the kinetics of I2 currents and accurately predicted the voltage dependence of peak conductance and steady state inactivation. It performed poorly, however, in predicting the increase in I2 current after trypsinization; in effect, the

Table 2. Fast and slow inactivation rate constants (sec^{-1}), all voltage-independent

Fast inactivation	NMG^+		Na^+	
	WT	I2	WT	I2
κ_o	215	292	315	319
γ_o	7	13	9	13
κ_c		320		596
γ_c		40		36
a		3		3
Slow inactivation	NMG^+ WTT	I2T	Na^+ WTT	I2T
κ	2.7	2.7	0.77	0.77
λ	0.056	0.056	0.015	0.015

Table 3. Peak current predicted in patches exposed to trypsin

Patch	Estimated N (post)	I peak (pA) measured (pre)	I peak (pA) predicted	Ratio meas/pred
Peak wildtype current at 0 mV as predicted by OSI model				
1209	17	7.27	8.9	0.82
1214	8	1.88	2.6	0.72
1229	685	270.0	277.5	0.97
0113	180	62.6	68.9	0.91
0118	86	28.8	39.6	0.73
Peak I2 current at 0 mV as predicted by MSI model				
010612	140	14.9	14.8	1.01
010613	340	28.3	36.8	0.77
010731	248	39.8	33.4	1.19
011223	24	4.42	3.8	1.16
011331	205	14.2	19.0	0.75
011441	770	56.2	24.8	2.27
122941	438	17.9	32.8	0.55

scheme still did not contain enough closed state inactivation to accurately describe the data. We found that also adding an inactivation transition from the final closed state C_{35} produced a scheme which much more accurately described the trypsin results while satisfying other constraints. This final, multiple state inactivation (MSI) model is the scheme we have used to describe inactivating I2 currents. As a preliminary scheme determined that inactivation from state C_{35} had to be fast to be effective, we constrained the transition from C_{35} to have rates $\kappa_c a$ and λ_c/a. These constraints allowed us to add six inactivation transitions with the use of only three free parameters. It should be emphasized that the MSI model does incorporate (and requires) inactivation from the open state determined by the voltage-independent rats κ_O and λ_O as before.

In contrast to the OSI model, the MSI model describes well the kinetics of I2 currents over a wide voltage range. This is demonstrated in Fig. 8*B* which compares OSI (dashed curves) and MSI (solid curves) in fitting the I2 current generated by a step to −10 mV. The relatively fast inactivation at −10 mV, which could not be fitted using OSI is well accounted for by the MSI model. Both schemes produce equivalent fits at +90 mV (Fig. 8*C*). A fit of the MSI model to currents over a range of depolarizations is also shown in Fig. 2*C*.

Based on the parameters which produced the best kinetic fits for I2 currents, the MSI model was used to predict the voltage dependence of peak conductance and steady state inactivation. As can be seen in Fig. 2*F*, the MSI scheme (dashed curve), does an excellent job of predicting the voltage dependence of the I2 peak conductance. As the data and fit are each normalized, only the shape of the curve tests the predictive power of the model. The voltage dependence of steady-state-inactivation (Fig. 2*E*) is predicted quite well, but not perfectly: there is a 5 mV offset between the data and the prediction at the midpoints of both curves.

Modeling the Effects of Trypsin

A critical test of the OSI and MSI models is their ability to predict the change in current magnitudes seen with the removal of inactivation by trypsin. The fitting of currents and the prediction of the amount of increased current after trypsin treatment was done as follows. Initially, pre- and post-trypsin records from a patch were fitted independently. The NI model was used for WT and I2 post-trypsin currents, the OSI model was used for pretrypsinized WT and the MSI model was used for pretrypsinized I2. On a patch-by-patch basis, there was little difference in the activation model parameters used for currents recorded before or after enzyme treatment for either WT or I2. An example of the fits of the three models to pre- and post-trypsinized WT and I2 currents is shown in Fig. 5.

To compare current magnitudes we made use of the least-squares fit that is performed to scale the model predictions to match experimental current time courses. The result of this fit of the NI model to a family of post-trypsin currents is an estimate of the number of channels *N* in the patch, along with the set of activation rate constants. Fixing these rate constants and given this estimate of *N*, the inactivating-current model (OSI for WT or MSI for I2) was then used to predict the peak current in the pretrypsin time course at a particular voltage. A comparison of the predicted and measured peak currents at 0 mV is presented in Table 3. In this analysis, we assume that trypsin treatment has no effect other than the removal of N-type inactivation.

Based on the data in the table, we see that for WT the OSI model consistently predicts too much current; for all but one patch there does not seem to be enough

inactivation in the OSI scheme, even when open-state inactivation rates are constrained by the decay of current in the same patch. For I2 the data scatter on both sides of the MSI prediction, with the median matching the prediction very well.

A more comprehensive way to check the models against the average behavior of trypsin-treated WT and I2 patches is to predict the change in shape and magnitude of the average conductance versus voltage curves (Fig. 6). As discussed above, changes in conductance curves are different for WT compared to I2; given that trypsin affects inactivation only, the differential changes will reflect the different inactivation processes. The OSI and MSI models were used to generate predicted conductance-voltage curves using the rates of inactivation obtained in fitting the kinetics of currents before trypsin treatment (Table 2). The NI model, using the rates in Table 1, was used to generate predicted conductance voltage curves for both WT and I2 after enzyme treatment.

Figure 6*B* indicates how well the MSI model does at predicting the average increase and change in shape of the I2 conductance-voltage relationship. While the individual patches showed large scatter, the model quite accurately predicts the average conductance increase over a wide voltage range. Figure 6*A* shows that the OSI model does much less well for WT, predicting too much peak conductance in the presence of inactivation (dotted curve in the figure).

The discrepancy in Fig. 6*A* and in Table 3 suggest that some closed-state inactivation might also be occurring in the WT channel. This is not surprising, because evidence for some closed-state inactivation in *Shaker* channels has been presented by Zagotta & Aldrich (1990). As a rough gauge of the amount of closed-state inactivation in the WT channel, we attempted to use the MSI scheme to predict the trypsin-induced change in WT conductance. As with I2, closed-state inactivation was constrained by the decay of WT currents before enzyme treatment. The decay kinetics of 4 of the 5 WT patches were in fact better accounted for by a version of the MSI model than with the OSI model (for example, see the dashed curve in Fig. 5*A;* rate constants are given in Figs. 5 and 6 legends). It should be kept in mind that this improvement may simply be due to the increased number of free parameters in the fits. As can be seen in Fig. 6*A* the MSI model underpredicted the overall peak conductance of pre-trypsin WT channels (dashed curve in Fig. 6*A*) by about the same amount as the OSI model overpredicted it.

The MSI scheme, using similar rates of closed state inactivation, significantly underpredicts the WT pretrypsin conductance yet accurately predicts the I2 peak conductance. To correctly predict the WT conductance change we would have to reduce the amount of closed-state inactivation compared to I2 values. Based on this result, we conclude there is much more significant inactivation from closed states in the I2 mutant compared to WT.

Discussion

Mutations that shift the voltage dependence of *Shaker* channel activation generally cause a parallel shift in the voltage dependence of inactivation. This has been observed with charge changes in the S4 region (Papazian et al., 1991) and also with substitutions of hydrophobic residues (Lopez, Jan & Jan, 1991; McCormack et al., 1993), and suggests that inactivation is tightly coupled to activation, deriving its voltage dependence from the activation process. An exception to this behavior is the I2 mutant channel, where a 45 mV shift in activation is accompanied by only a 9 mV shift in inactivation. We have presented several lines of evidence that inactivation in the I2 channel is more complete and more rapid than in the WT channel, and conclude that inactivation can proceed before the channel is fully activated. The evidence includes the following:

First, a comparison of steady-state behavior shows that I2 inactivation is much more complete at lower levels of activation than is seen in the WT channel (Fig. 3*A*), and is much more complete than expected from a simply theory of open-state inactivation. Second, a simple prediction for the voltage dependence of the inactivation time constant was applied to WT and I2 currents. The prediction was based on the assumption of open-state inactivation, and was seen to hold for WT channels but not for I2 (Fig. 3*B, C*). Third, the effect of inactivation removal by trypsin was examined. Trypsin was applied to the cytosolic aspect of macropatches, and caused an increase of mean current through both WT and I2 channels (Figs. 5 and 6). The larger increase for I2 compared to WT, despite similar inactivation time constants at large depolarizations, leads us to the conclusion that I2 channels are more likely than WT to inactivate before opening.

Finally, with an extensive kinetic model that incorporates the inactivation process into a recent model of activation, it was found that inactivation from closed states is required to describe I2 kinetics. This multiple-state inactivation (MSI) model also completely accounts for the increase in I2 current after trypsin treatment, while the OSI model, which incorporates only inactivation from the open state, fails to describe the kinetics or the current increase. On the other hand, the OSI scheme adequately describes WT current kinetics, but a discrepancy in its predicted current after trypsin suggests that additional inactivation pathways may be present for WT channels as well.

It is instructive to consider the ways in which inac-

tivation transitions have been characterized previously in voltage-gated channels. First, consider the phenomenon of open-state recovery from inactivation. If a channel inactivates only from the open state, it is expected to be able to close only after recovering from inactivation. Tail currents arising from partial recovery through open states have been seen in *Shaker*-subfamily channels (Demo & Yellen, 1991; Ruppersberg et al., 1991). We did not examine such tail currents in I2; a comparison with WT is complicated by the more rapid deactivation in I2 channels. Interestingly, while Demo and Yellen concluded that *Shaker* did not inactivate without prior opening, correlating with their demonstration of open channel recovery from inactivation, they also showed that channels occasionally recovered from inactivation without channel opening.

Closed-state inactivation can, in principle, be characterized in single-channel recordings using a double-pulse protocol (Aldrich, Corey & Stevens, 1983; Aldrich & Stevens, 1983) or by searching for single-channel traces without openings (Zagotta & Aldrich, 1990; Demo & Yellen, 1991). The interpretation of these experiments can be confounded, however, by slow inactivation processes which cause failures in channel opening. These failures are essentially indistinguishable from those caused by closed-state inactivation.

As an alternative to these methodologies, we used trypsin treatment to remove inactivation from the channels under study. Since it appears specifically to affect the fast inactivation process, this treatment is perhaps a more reliable test of the degree of inactivation in channels than are the corresponding single-channel experiments. Because we make a macroscopic current measure, slow inactivation or other processes of channel ''hibernation'' appear as reductions in current which are presumably present in both the trypsin-treated and pretreated channels and are therefore nonconfounding.

Limits on Data and Modeling Results

It is appropriate to discuss factors inherent in both the data and the modeling which may limit the interpretations we have given here. First, if trypsin has the effect of making channels nonfunctional as well as removing inactivation, then the results of trypsin experiments and its prediction by the OSI and MSI models have to be regarded as qualitative rather than quantitative proof of closed state inactivation. In control experiments we found that trypsin treatment causes little change in the current through noninactivating channels (Fig. 4) and that channel currents remain stable after trypsin treatment (*see* Materials and Methods). It should be noted that, if a fraction of channels is made nonfunctional by the trypsin application, then the larger increase in I2 current with trypsin treatment reflects an even more dramatic removal of closed-state inactivation than we have modeled here.

Second, it should be emphasized that the model we have used for channel activation has not been rigorously established for I2 channels. We have not collected gating currents and single-channel data which would serve to more completely constrain the activation related parameters of the NI model. Nevertheless, the MSI model, derived from the NI model, is quite successful in describing the behavior of I2 channels. The only piece of data that is not well accounted for is I2's steady-state inactivation voltage dependence (Fig. 2*E*). The largest part of the error in the fit, namely the 5–10 mV offset, can be accounted for by making a small alteration in the activation rates. However, even when the offset is corrected, the data and the model prediction are still not identical. We tried other schemes, both with and without closed state inactivation, in a further attempt to fit simultaneously the steady-state inactivation along with kinetics, voltage dependence of peak current and the trypsin results; all were inadequate in some measure. It may be instructive to briefly describe some of these deficient schemes and how they failed.

In one set of schemes we experimented with allowing closed state inactivation from more fully closed subunit states, i.e, S0, S1 or S2 (*see* Fig. 7*A*) rather than from S3. The thought was that the voltage dependence of steady state inactivation may have been a function of states further from the open state. As might be expected, none of these could describe current decay as the closed-to-inactivated transition is too far away from the open state. In another variant scheme we relaxed the geometric progression of inactivation rate constants. Within a scheme with inactivation transitions from C34 and C35 only, we allowed independent forward and backward rates for each closed to inactivated transition. This scheme did about as well as the MSI model, but did not improve the fit of steady-state inactivation. Interestingly, the values found for the completely unlinked rates come close to the MSI rates forced by the multiplicative factor.

All kinetic modeling is by nature tentative. While open-state inactivation models clearly cannot account for I2 behavior, we present the MSI model here as an ''existence proof'' of a model that can account relatively well for I2 behavior.

Function and Structure of Close-state Inactivation

The increased closed-state inactivation in I2 can be imagined to arise by two different mechanisms. First, the mutation could have a direct effect in allowing new transitions to occur between closed states and inactivated states; specifically, the I2 mutation could be imagined to

change the binding site for the inactivation ''ball'' so that binding can occur more readily while the channel is in closed states. Alternatively, the increased closed-state inactivation could arise indirectly, as a consequence of changes in the activation process which increase the occupancy of certain closed states. In this case inactivation would be possible from these states even in the WT channel; however, only in the mutant are these states long lived enough for the ball binding reaction to occur.

We strongly favor the first of these hypotheses primarily because of the behavior of the other substitutions of L382 (Fig. 1). In V2T, where the activation process has been most carefully studied, the closed states just prior to opening are greatly stabilized, and have much higher occupancies than in WTT channels. This is the primary means by which the activation midpoint of the curve is shifted in a positive direction (Schoppa et al. 1991; Schoppa & Sigworth, 1997). If the closed-state inactivation that we measure were solely a result of increased occupancy of states prior to opening, then we would predict more closed-state inactivation in V2 than in I2, because I2s shift in activation gating is smaller. As it turns out, V2 and the other substitutions at L382 follow a pattern of shifts in activation and inactivation midpoints that parallels WT. The I2 mutation is an exception, and appears to have a unique effect on inactivation transitions.

Sodium channels are able to inactivate without opening (Horn, Patlak & Stevens, 1981; Horn & Vandenberg, 1984; Vandenberg & Horn, 1984; Vandenberg & Bezanilla, 1991). This is an important property for channels that provide the inward current for fast action potentials. Closed-state inactivation allows sodium channels to remain closed during gradual depolarizations, preventing action potential generation. Perhaps more importantly, closed-state inactivation pathways allow sodium channels to recover from inactivation without opening, preventing afterdepolarizations that could give rise to undesirable repetitive firing in excitable cells (Kuo & Bean, 1994). A-type potassium channels, such as *Shaker,* do not need these safeguards against channel opening, and in their role of controlling the firing frequency of neurons (Connor, 1978) it might be argued that inactivation primarily from the open state produces a more linear current-frequency relationship for repetitive firing of neurons. It is interesting, then, that the effect of the I2 mutation is to change the behavior of *Shaker* channels to make them more like sodium channels.[1]

The site of the I2 mutation, L382 in the *Shaker* B sequence, appears to participate in conformational changes associated with channel opening. Mutations at this position shift the voltage dependence of channel activation (McCormack et al., 1991; 1993), and such shifts can be explained by a change in the equilibrium of a late step in the activation process (Schoppa et al., 1992). The magnitude and rank order of the shifts induced by different substitutions at this position suggest that the environment of this residue changes in the process of channel activation, becoming less polar with channel opening (Sigworth, 1994). Further, Holmgren, Jurman & Yellen (1996) have demonstrated voltage- and time-dependent accessibility of a cysteine residue at this position, consistent with the idea that the side-chain of this residue becomes accessible to the intracellular environment during an intermediate state that precedes channel opening.

It is not unexpected that a residue that participates in channel opening would also affect the inactivation process, especially in view of the proximity of L382 to residues that have previously been implicated in N-type inactivation. Isacoff et al. (1991) have shown that nearby residues in the S4-S5 linker region of *Shaker* B, at positions 385, 388, 392, 395 and 396, also influence the inactivation properties. Mutations at L385, like I2, produce faster and more complete inactivation. More recently Holmgren et al. (1996) have identified position 391 as an important residue that can interact electrostatically with an inactivation ball, presumably as part of its receptor site.

We thank Chang Wang, Yun-gui Tang and Leon Islas for comments on the manuscript. This work was supported by National Institutes of Health grant number NS-21501.

References

Aldrich, R.W., Stevens, C.F. 1983. Inactivation of open and closed sodium channels determined separately. *Cold Spring Harb. Symp. quant. Biol.* **48:**147–153

Aldrich, R.W., Corey, D.P., Stevens, C.F. 1983. A reinterpretation of mammalian sodium channel gating based on single channel recording. *Nature* **306:**436–441

Baukrowitz, T., Yellen, G. 1995. Modulation of K^+ current by frequency and external $[K^+]$: a tale of two inactivation mechanisms. *Neuron.* **15:**951–960

Bezanilla, F., Armstrong, C.M. 1977. Inactivation of the sodium channel. I. Sodium current experiments. *J. Gen. Physiol.* **70:**549–566

Benzanilla, F., Perozo, E., Stefani, E. 1994. Gating of *Shaker* channels. II. The components of gating currents and a model of channel activation. *Biophys. J.* **66:**1011–1021

Connor, J.A. 1978. Slow repetitive firing from fast conductance changes in neurons. *Fed. Proc.* **37:**2139–2145

Choi, K.L., Aldrich, R.W., Yellen, C. 1991. Tetraethyl ammonium blockade distinguishes two inactivation mechanisms in voltage-activated K^+ channels. *Proc. Natl. Acad. Sci. USA* **88:**5092–5095

Colquhoun, D., Hawkes, A. 1995. A Q-matrix cookbook. How to write only one program to calculate the single-channel and macroscopic predictions for any kinetic mechanism. *Single-Channel Recording.* B. Sakmann and E. Neher, eds. pp. 589–633. Plenum, New York

[1] Indeed, Domain IV of most sodium channels has an isoleucine at what appears to be the equivalent position to L382.

Demo, S.D., Yellen, G. 1991. The inactivation gate of the *Shaker* K^+ channel behaves like an open-channel blocker. *Neuron* **7:**743–753

Gomez-Lagunas, F., Armstrong, C.M. 1995. Inactivation in *ShakerB* K^+ channels: a test for the number of inactivation particles on each channel. *Biophys. J.* **68:**89–95

Hille, B. 1992. Ionic Channels of Excitable Membranes. Sinauer Associates, Sunderland MA

Holmgren, M., Jurman, M.E., Yellen, G. 1996. N-type inactivation and the S4-S5 region of the Shaker K^+ channel. *J. Gen. Physiol.* **108:**195–206

Horn, R., Patlak, J., Stevens, C.F. 1981. Sodium channels need not open before they inactivate. *Nature* **291:**426–427

Horn, R., Vandenberg, C.A. 1984. Statistical Properties of Sodium channels. *J. Gen. Physiol.* **84:**505–534

Hoshi, T., Zagotta, W.N., Aldrich, R.W. 1990. Biophysical and molecular mechanisms of *Shaker* potassium channel inactivation. *Science* **205:**533–538

Hoshi, T., Zagotta, W.N., Aldrich, R.W. 1991. Two types of inactivation in *Shaker* K^+ channels: effects of alterations in the carboxyl-terminal region. *Neurons* **7:**547–556

Isacoff, E., Jan., Y.N., Jan, L.Y. 1991. Putative receptor for the cytoplasmic inactivation gate in the *Shaker* K^+ channel. *Nature* **353:**86–90

Iverson, L.E., Rudy, B. 1990. The role of divergent amino and carboxyl domains in the inactivation properties of potassium channels derived from the *Shaker* gene of *Drosophila. J. Neurosci.* **10:**2903-2916

Kamb, A., J. Tseng-Crank and M.A. Tanouye. 1988. Multiple products of the Drosophila *Shaker* gene may contribute to potassium channel diversity. *Neuron* **1:**421–30

Kuo, C-C., Bean, B.P. 1994. Na^+ channels must deactivate to recover from inactivation. *Neuron* **12:**819–829

Lopez, G.A., Jan, Y.N., Jan, L.Y. 1991. Hydrophobic substitution mutations in the S4 sequence alter voltage-dependent gating in *Shaker* K^+ channels. *Neuron* **7:**327–36

Lopez-Barneo, J., Hoshi, T., Heinemann, S.H., Aldrich, R.W. 1993. Effects of external cations and mutations in the pore region on C-type inactivation of *Shaker* potassium channels. *Receptors and Channels* **1:**61–71

McCormack, K., Joiner, W.J., Heinemann, S.H. 1994. A characterization of the activating structural rearrangements in voltage-dependent *Shaker* K^+ channels. *Neuron* **12:**301–15

McCormack, K., Lin, L., Sigworth, F.J. 1993. Substitution of a hydrophobic residue alters the conformational stability of *Shaker* K^+ channels during gating and assembly. *Biophys. J.* **65:**1740–1748

McCormack, K., Tanouye, M.A., Iverson, L.E., Lin, J., Ramaswami, M., McCormack, T., Campanelli, J.T., Mathew, M.K., Rudy, B. 1991. A role for hydrophobic residues in the voltage-dependent gating of *Shaker* K^+ channels. *Proc. Natl. Acad. Sci. USA* **88:**2931–2935

Papazian, D.M., Timpe, L.C., Jan, Y.N., Jan, L.Y. 1991. Alteration of voltage-dependence of Shaker potassium channel by mutations in the S4 sequence. *Nature* **349:**305–10

Rudy, B., Iverson, L.E. 1992. Ion Channels. Methods in Enzymology, volume 207. Academic Press, San Diego

Ruppersberg, J.P., Frank, R., Pongs, O., Stocker, M. 1991. Cloned neuronal I_K(A) channels reopen during recovery from inactivation. *Nature* **353:**657–660

Schoppa, N.E., McCormack, K., Tanouye, M.A., Sigworth, F.J. 1992. The size of gating charge in wild-type and mutant *Shaker* potassium channels. *Science* **255:**1712–1715

Schoppa, N.E., Sigworth, F.J. 1997. Activation of *Shaker* potassium channels. I. Characterization of voltage-dependent transitions. Submitted

Schwarz, T.L., Temple, B.L., Papazian, D.M., Jan, Y.N., Jan, L.Y. 1988. Multiple potassium-channel components are produced by alternative splicing at the *Shaker* locus in *Drosophila. Nature* **331:**137–141

Sigworth, F.J. 1994. Voltage gating of ion channels. *Q. Rev. Biophys.* **27:**1–40

Vandenberg, C.A., Bezanilla, F. 1991. A sodium channel gating model based on single channel, macroscopic ionic, and gating currents in the squid giant axon. *Biophys. J.* **60:**1511–1533

Vandenberg, C.A., Horn, R. 1984. Inactivation viewed through single sodium channels. *J. Gen. Physiol.* **84:**535–564

Zagotta, W.N., Aldrich, R.W. 1990. Voltage-dependent gating of *Shaker* A-type potassium channels in *Drosophila* muscle. *J. Gen. Physiol.* **95:**29–60

Zagotta, W.N., Hoshi, T., Aldrich, R.W. 1989. Gating of single *Shaker* potassium channels in *Drosophila* muscle and in *Xenopus* oocytes injected with *Shaker* mRNA. *Proc. Natl. Acad. Sci. USA* **86:**7243–7247

Zagotta, W.N., Hoshi, T., Aldrich, R.W. 1994. *Shaker* potassium channel gating III: Evaluation of kinetic models for activation. *J. Gen. Physiol.* **103:**321–362